

# Preparation and Properties of Shape Memory PEG/IEM Resin and Its Composite Designed for Ureter Stent

Ce Li, Fenghua Zhang, Wei Zhao, Linlin Wang, Yanju Liu, and Jinsong Leng\*

In this paper, isocyanatoethyl methacrylate (IEM) is used to functionalize the two ends of poly(ethylene glycol) (PEG) diol with acrylic acid groups through an urethanization reaction. The synthesized PEG/IEM resin is then photo-cured with a 405 nm ultraviolet lamp.  $T_{\text{trans}}$  of the PEG/IEM resin can be regulated by the different molecular weights of PEG and the use of plasticizer Triacetin to reach 44 °C, which is closer to the human body temperature. Cytotoxicity assay and DMA shape memory cycling testing show that the PEG/IEM resin has excellent biocompatibility and shape memory properties. The flower structure is prepared and its shape recovery process is demonstrated. The performance of 10wt% nano  $\text{Fe}_3\text{O}_4$ /PEG4000/IEM resin and its composite spring stent structure satisfy the requirement of the stent properties in vivo, and can quickly recover to the original shape under magnetically driven. This work provides a material option for developing new biological application devices such as ureter stents.

shape, which was fabricated during the forming process.<sup>[11]</sup> Subsequently, heat the SMP to the transition temperature (glass transition temperature, melting temperature, or crystallization-melting temperature), and the phase transformations occur in SMP internal structures. During this process, the SMP could be fixed to a temporary shape. Then, cool down the temperature, the internal molecular chains are frozen and the generated stress is stored, promoting the preservation of temporary shape.<sup>[12]</sup> Finally, heat the SMP with the temporary shape up to the transition temperature again, the phase transformations occur, and the internal stress stored before is released. As a result, the SMP spontaneously recovers its original shape.<sup>[13]</sup> Due to the unique programmable deformation ability,<sup>[14,15]</sup> SMPs have broad application prospects for biomedical stents,<sup>[16]</sup> flexible electronics,<sup>[17]</sup> and smart robots.<sup>[18]</sup>

## 1. Introduction

Shape memory polymers (SMPs), as novel smart materials, could memorize pre-designed temporary shapes<sup>[1]</sup> and retain the original shape upon the corresponding stimuli,<sup>[2]</sup> including heat,<sup>[3]</sup> electricity,<sup>[4]</sup> magnetism,<sup>[5]</sup> light,<sup>[6]</sup> and so on. Take heat-triggered SMP as an example, the matrix polymer usually contains two parts: reversible phase and rigid phase. The former commonly includes flexible segments and an amorphous phase, which could memorize the deformed temporary shape. The latter usually includes rigid segments,<sup>[7]</sup> crystalline phase,<sup>[8]</sup> and entanglements,<sup>[9]</sup> which could maintain and retain the original shape.<sup>[10]</sup> Initially, the SMP exhibits the original stable


In recent years, the combination of the unique deformation-recovery ability and excellent biological performances has attracted much attention, and the SMPs based on biocompatible materials (polylactic acid,<sup>[19,20]</sup> polyurethane,<sup>[21,22]</sup> polyacrylic acid,<sup>[23,24]</sup> etc.) matrix have broadly used as implanted stents, tissues, and occluders.<sup>[25]</sup> At present, ureter stricture has become common trouble for males,<sup>[26]</sup> which could be concerned by the scarring, causing from that the scar tissue replaces the spongy tissue.<sup>[27]</sup> The commonly used treatment method for these ureter canal narrowing is implanted stents, which commonly use metal as the material matrix. Nevertheless, due to biocompatibility, biodegradability, easy processing, and low cost, polymer materials have been integrated into the fabrication and manipulation of ureter strictures.<sup>[28]</sup> Besides, combined with the programmable deformation-recovery ability of SMPs,<sup>[29]</sup> the SMPs could satisfy the minimally invasive implantable therapy for ureter stricture, exhibiting the broad using potential.<sup>[30]</sup>

The development and application of acrylic resin in the medical field have a long history. In 1936, the German Kulzerr company began to sell tooth adhesive with methyl methacrylate (MMA) as the main body; in 1959, Fastman910a methyl cyanoacrylate fast adhesive was invented in the United States, realizing the revolution of a surgical operation from suture to bonding; in 1960, Charnly first successfully used acrylic bone cement in the operation of the artificial hip joint. With the rapid development of medical polymer materials, the research, development, and application of medical acrylic resin are also expanding. The medical adhesive based on a-cyanoacrylate alone has been used

C. Li, F. Zhang, L. Wang  
Centre for Composite Materials and Structures  
Harbin Institute of Technology (HIT)  
No. 2 Yikuang Street, Harbin 150080, P. R. China

W. Zhao, Y. Liu  
Department of Astronautical Science and Mechanics  
Harbin Institute of Technology (HIT)  
No. 92 West Dazhi Street, Harbin 150001, P. R. China

J. Leng  
Centre for Composite Materials and Structures  
Harbin Institute of Technology (HIT)  
No. 2 Yikuang Street, Harbin 150080, P. R. China  
E-mail: yj\_liu@hit.edu.cn

 The ORCID identification number(s) for the author(s) of this article can be found under <https://doi.org/10.1002/adhm.202300400>

DOI: 10.1002/adhm.202300400

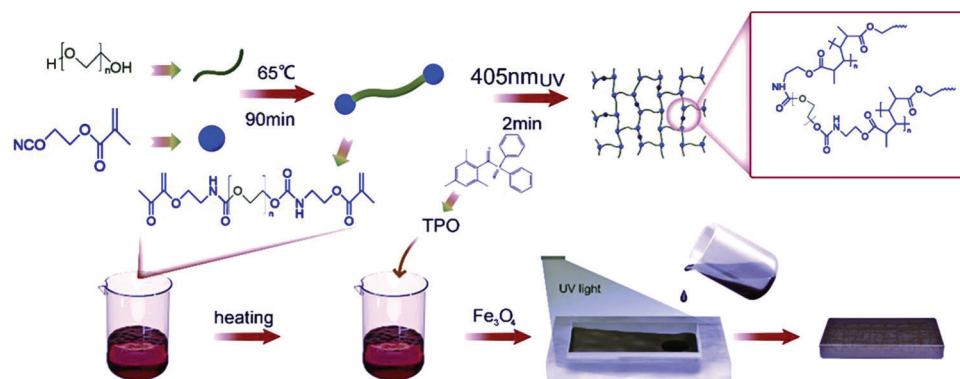


**Figure 1.** Schematic diagram of the overall research process of this paper and Synthetic route of UV-cured PEG/IEM resin.

in more than 1 million cases. Medical acrylic resin has gradually realized product serialization and variety diversification, which is used in many scenes.

Today, acrylic materials combined with shape memory and biological applications are gradually becoming a research hotspot. Kim used a simple melt-mixing method to manufacture epoxidized natural rubber (ENR)/poly(ethylene acrylic acid copolymer) (EAA)/PCL ternary blends, which has triple shape memory behavior and can be crosslinked without any additional crosslinking agent at high temperature as a promising shape memory material in many aerospace and in vivo applications.<sup>[31]</sup> Huang grafted acrylic acid onto polycaprolactone (PCL) and then melt-blended the grafted PCL and natural rubber (NR) to form PCL/NR blends. The prepared blend has good biological descriptiveness and shape memory effect making its self-healing performance excellent.<sup>[32]</sup> Wan synthesized  $\text{Fe}_3\text{O}_4$ -g-P(TMA-co-LA-co-VI) with near-infrared light, magnetic, self-healing, and thermal multiple-stimulated shape memory performance. It has a bright future in the application of intelligent life science.<sup>[33]</sup> Fulati reported a novel design of customizable 4bPCL-based SMP strings with different mechanical properties. The SMP strings developed were very promising in future applications such as the treatment of aneurysms and minimally invasive fetal surgery.<sup>[34]</sup> Liu developed an elastic 3D porous PLA/SiO<sub>2</sub> composite nanofibrous aerogel scaffold. The composite-induced rabbit bone marrow stem cells (rBMSCs) promoted bone repair and osteoblasts, which may have great guidance for tissue engineering.<sup>[35]</sup> Wiley designed hydrogels formed by a photo-initiated thiol-ene reaction between a dually enzymatically degradable peptide linker and multiarm polyethylene glycol. This work has created a hydrogel-based synthetic material system and design rules for sequential mechanical property control using orthogonal triggers of enzymes and applied light.<sup>[36]</sup>

In this paper, a series of poly(ethylene glycol) (PEG)/isocyanatoethyl methacrylate (IEM) resins were synthesized by the UV radiation curing method. PEG, due to its excellent biological performances,<sup>[37]</sup> deformation ability, and the transition temperature close to the human body temperature,<sup>[38]</sup> has been widely used in smart biomedical applications.<sup>[39]</sup> This paper makes up for the research blank of acrylic material in the soft material required by the ureter stent. The prepared resin has good biocompatibility, and the shape memory effect of its composite can be

**Table 1.** Average molecular weight and molecular weight distribution of PEG and PEG/IEM resin.

Test sample	Average molecular weight [ $M_n$ ] [ $\text{g mol}^{-1}$ ]	Molecular weight distribution
PEG4000	3900	1.15
PEG4000/IEM	3192	1.22
PEG6000	5142	1.22
PEG6000/IEM	5039	1.22
PEG8000	6595	1.27
PEG8000/IEM	6190	1.33

driven remotely by a magnet, which is suitable for in vivo application scenarios.

## 2. Results and Discussion

### 2.1. Synthesis and Characterization of PEG/IEM Resins

The schematic diagram of the overall research process of this paper and the synthetic route of UV-cured PEG/IEM is shown in **Figure 1**. The average molecular weights and their distributions of PEG (molecular weight 4000, 6000, 8000) and the synthesized PEG/IEM resins were tested by gel permeation chromatography (GPC). The test results are shown in **Table 1**.

The average molecular weights ( $M_n$ ) of the PEG/IEM resin decrease compared with the average molecular weights of raw PEG. The molecular weight distribution coefficients of the PEG/IEM resin increase slightly meaning the molecular weight distributions get wider, which may be caused by incomplete reactions of PEG and IEM. The molecular weight of IEM is much lower than that of PEG. Due to the incomplete reaction, the sample PEG4000/IEM contains four substances: IEM, PEG4000, 1PEG4000-1IEM (product of the reaction between one PEG molecule and one IEM molecule), and 1PEG4000-2IEM (product of the reaction between one PEG molecule and two IEM molecules). The sample PEG4000/IEM is a complex mixture, therefore, the molecular distribution of PEG4000/IEM is wider than that of PEG4000.

The <sup>1</sup>H NMR spectra test of raw PEG and synthesized PEG/IEM resin was carried out.  $(\text{CD}_3)_2\text{SO}$  was used as a solvent.

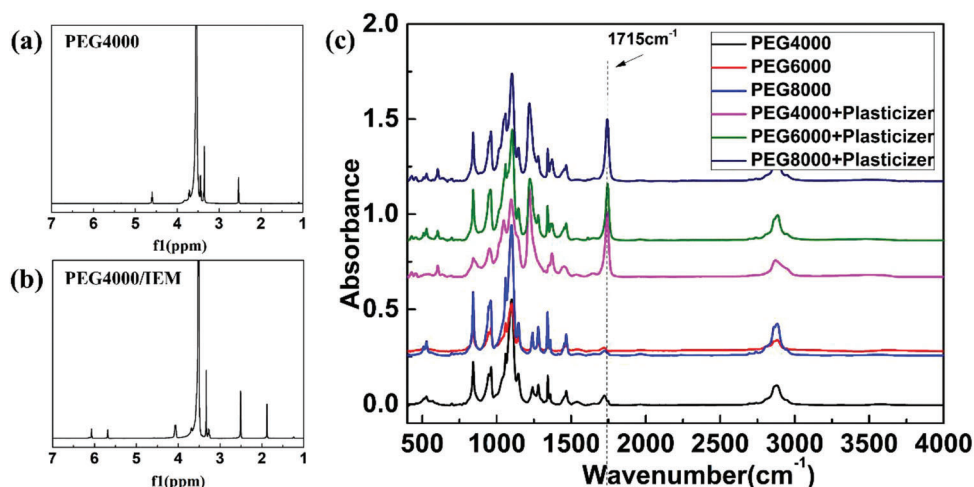


**Figure 2.** a)  $^1\text{H}$  NMR test results of raw PEG and the b) synthesized PEG4000/IEM resin; c) FT-IR analysis of the cured PEG/IEM resin with different molecular weights before and after plasticization.

The test equipment used was Bruker Avance III 400 MHz NMR with Autosampler. The  $^1\text{H}$  NMR test results of raw PEG ( $M_n=4000$ ) before synthesis are shown in **Figure 2a**. The strongest resonance appeared at the chemical shift of 3.54 ppm, which was the resonance of  $^1\text{H}$  on  $-\text{CH}_2$  in the PEG repeating unit. Due to the large amount of  $^1\text{H}$ , this peak masked resonance of the others. The resonance peak of  $^1\text{H}$  on  $-\text{CH}_2$  adjacent to the end group is shifted to 3.35 ppm due to the influence of the end group. The solvent resonance was located at the chemical shift of 2.54 ppm, and the resonance of  $^1\text{H}$  in  $-\text{OH}$  was located at 4.6 ppm.

The NMR test results of the synthesized PEG4000/IEM resin are shown in **Figure 2b**. The resonance of  $^1\text{H}$  on  $-\text{CH}_2$  in PEG still occupied an absolute advantage, masking the resonance peak of other  $^1\text{H}$ . The chemical shift remains unchanged at 3.54 ppm. The resonance peak of  $^1\text{H}$  on  $-\text{CH}_2$  adjacent to the end group is shifted to 3.35 ppm due to the influence of the end group. The resonance at 4.60 ppm disappeared, which proved that the  $-\text{OH}$  group reacted completely and the synthesis was complete. The resonance of  $-\text{CH}_3$  in the methacrylic acid group was at 1.91 ppm; 4.09 ppm was the resonance of two  $^1\text{H}$  on the double bond  $-\text{CH}_2$  in the methacrylic acid group; 7.44 ppm was the resonance of  $^1\text{H}$  in  $-\text{NH}$ ; 6.10 and 5.71 ppm were the resonance of two  $-\text{CH}_2$  connected between the methacrylic acid group and  $-\text{NH}$  group. The NMR results showed that the synthesis reaction was smooth and complete, and the product had fewer impurities.

The group changes during the synthesis and curing of the cured PEG/IEM resin were characterized by Fourier transform-Infrared spectroscopy (FT-IR) analysis. As shown in **Figure 2c**, the absorption band at  $2275\text{--}2240\text{cm}^{-1}$  of the  $-\text{N}=\text{C}=\text{O}$  group disappeared, indicating that IEM reacted completely without residue. There was a new band of carbamate at  $1715\text{cm}^{-1}$ , and the alcohol  $-\text{OH}$  band disappeared at  $3313\text{cm}^{-1}$ , the stretching vibration band corresponding to  $-\text{CH}_2$  from IEM and PEG were at  $2883\text{cm}^{-1}$ . The above showed that PEG and IEM were successfully synthesized and the required UV-curable PEG/IEM resin was obtained; The band of  $-\text{C}=\text{C}=\text{O}$  in methacrylic acid at  $2150\text{cm}^{-1}$  disappeared, indicating that the double bonds were completely reacted and the PEG/IEM resin was entirely cured

**Table 2.** Test results of gel content of PEG/IEM resin.

Test sample	Gel content[%]
PEG4000/IEM	98.52
PEG6000/IEM	99.50
PEG8000/IEM	99.98

under UV light. The enhancement of the ester group band at  $1715\text{cm}^{-1}$  after plasticization resulted from the superposition of the ester group bands from plasticizer glycerol triacetate and carbamate.

The raw PEG and the synthesized PEG/IEM resin were analyzed by X-ray diffraction (XRD) to investigate the crystallinity. The XRD curve obtained is shown in **Figure S1**, Supporting Information. Sample numbers 1–3 represent raw PEG with molecular weights of 4000, 6000, and 8000; sample numbers 4–6 represent corresponding PEG4000/IEM, PEG6000/IEM, and PEG8000/IEM resins respectively. The diffraction peaks of the six samples matched well with the standard diffraction pattern (PDF#49-2095). It was shown that the synthesis did not change the crystalline property of PEG, and the shape memory effect of PEG/IEM resin was due to the melting and recrystallization of semi-crystals in PEG.

The gel content of the PEG/IEM resin was tested to ensure that UV curing crosslinking reached a high level. The columnar samples of PEG/IEM resins (PEG with  $M_n=4000$ , 6000, and 8000) were cured under UV irradiation for 5 min. To determine the gel content, samples with mass  $m_0$  were placed in solvent ethanol for 24 h at  $25^\circ\text{C}$ . After extraction, the swollen samples were dried to the final mass ( $m_d$ ). The gel content (G) value was got using the equation:  $G = m_d/m_0 \times 100\%$ . Test results are shown in **Table 2**. According to the results, the gel content of the cured PEG/IEM resins with different molecular weights could reach more than 98%, and the cross-linking degree was high.

The heat transition of UV-cured PEG/IEM resins with different molecular weights and their plasticized resins was analyzed

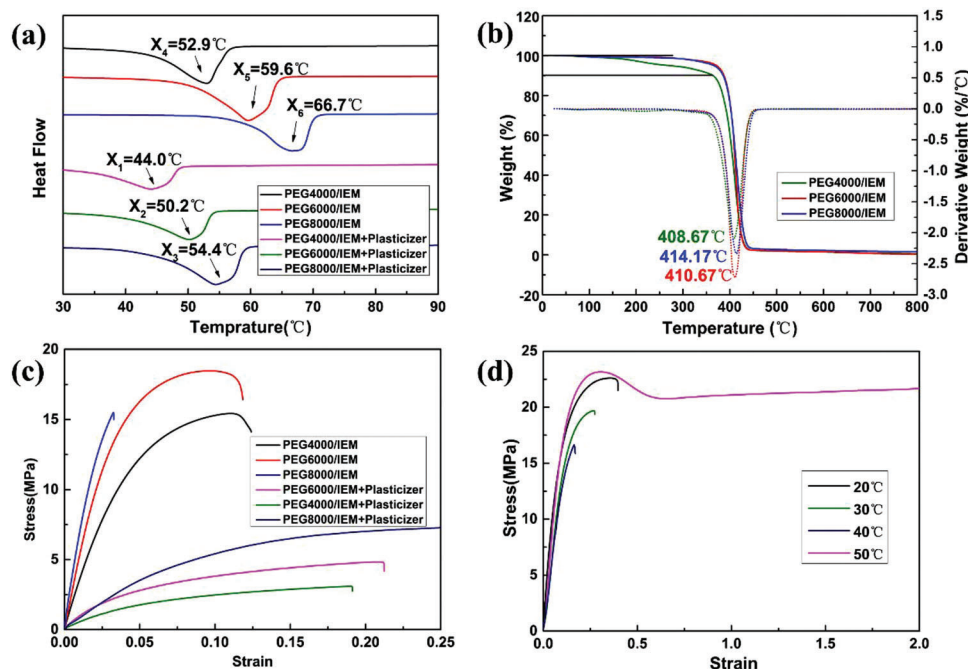


**Figure 3.** a) DSC curves of the UV-cured PEG/IEM resins with different molecular weights before and after plasticization; b) TGA test result curves of the UV-cured PEG/IEM resins with different molecular weights of PEG ( $M_n=4000$ , 6000, and 8000); c) Stress-strain curves of the UV-cured PEG/IEM resins with different molecular weights of PEG ( $M_n=4000$ , 6000, and 8000) before and after plasticized; d) Stress-strain curves of the UV-cured PEG/IEM resins with raw PEG molecular weight of 4000 at different temperatures.

by DSC. The curve of test results is shown in **Figure 3a**. The peak value of the curve represents the melting temperature  $T_m$  of resin semi-crystallization. The temperature also reflects the shape memory recovery temperature of PEG/IEM resins. According to the results, the transition temperatures of UV-cured PEG/IEM resins with  $M_n$  of 4000, 6000, and 8000 before plasticization were 52.9, 59.6, and 66.7 °C, respectively. After plasticization by 30wt% triacetate, the transition temperatures decreased to 44.0, 50.5, and 54.4 °C, respectively. The melting temperature of PEG/IEM resin gradually decreased with the decrease in molecular weight of raw PEG. Meanwhile, the melting temperature could be decreased more obviously by plasticization. By changing the plasticization and molecular weight of raw PEG, the shape memory recovery temperature of UV-cured PEG/IEM resin could be regulated. Therefore, the thermal property of UV-cured PEG/IEM resin and the prepared devices can be adjusted and selected according to the specific requirements of biological applications.

Thermogravimetric analysis (TGA) was carried out on the UV-cured PEG/IEM resins with different molecular weights of PEG ( $M_n=4000$ , 6000, and 8000). The result curves in **Figure 3b** showed that the thermal weight loss had two stages: the first was the weight loss of free water and other small molecules; then the second was the weight loss of resin itself. It could be seen that the small molecular weight part of the UV-cured PEG4000/IEM resin was relatively large, indicating that the increase of PEG molecular weight was beneficial to the rise of gel content. All the resins were thermally decomposed at last without residue. The DTG curves of the UV-cured PEG/IEM resins were obtained by calculating the first derivative of TGA result curves.

According to the curves, the maximum thermal decomposition temperatures of the UV-cured PEG/IEM resins were 408.67, 410.67, and 414.17 °C when the average molecules of PEG were 4000, 6000, and 8000, respectively. This indicated that with the increase of PEG molecular weight, the maximum thermal decomposition temperature of the UV-cured PEG/IEM resins increased slightly.

The static mechanical tensile tests of the UV-cured PEG/IEM resins with different molecular weights of PEG ( $M_n=4000$ , 6000, and 8000) and their plasticized resins were carried out. The stress-strain curves obtained are shown in **Figure 3c**. The elastic modulus of the UV-cured PEG/IEM resins with different molecular weights of PEG ( $M_n=4000$ , 6000, and 8000) before plasticization at a strain of 0.01 were 359.6, 530.9, and 694.6 MPa, respectively, which could tell that the elastic modulus decreases gradually with the decrease of raw PEG molecular weight used. After plasticized by 30wt% triacetate, the elastic modulus of the UV-cured PEG/IEM resins with different molecular weights of PEG ( $M_n=4000$ , 6000, and 8000) at a strain of 0.01 decreased to 55.7, 97.9, and 177.08 MPa respectively. Plasticization decreased the elastic modulus of the UV-cured PEG/IEM resins decrease while the toughness of the UV-cured PEG/IEM resins was enhanced. When the molecular weight of raw PEG was 8000, the toughness of the UV-cured PEG/IEM resins was lower than 4000 or 6000. But although the elastic modulus was higher, the increase of brittleness might limit the application prospect of the UV-cured PEG/IEM resins under raw PEG molecular weight of 8000.

**Figure 3d** shows the stress-strain curves of the UV-cured PEG/IEM resins with raw PEG molecular weight of 4000 at



different temperatures. As the curve showed, the elastic modulus (at strain 0.15) at 20, 30, 40, and 50 °C were 129.7, 115.0, 107.5, and 135.4 MPa respectively. Before the crystalline melting temperature, the elastic modulus of the UV-cured PEG/IEM resin decreased slightly with the increase in temperature, while after the crystalline melting temperature, the elastic modulus increased slightly again. Due to the strong water absorption of the PEG/IEM resin sample, the water acts as a part of the plasticizer. At 50 °C, the water absorbed by the sample is partially removed, and the plasticizing effect decreases, so the modulus slightly increases at 50 °C. The resin showed the characteristics of general plastic material when it is far away from the crystalline melting temperature, that is, the temperature of shape recovery; when the temperature was close to  $T_m$ , the resin had a high elastic deformation stage that did not exist before (after strain 0.5). This characteristic of the UV-cured PEG/IEM resin could realize its functionality in biological applications.

According to regulations for plasticizers in GB 9685-2008, the content of the plasticizer is generally not more than 40% wt. The DSC and mechanical property tests of PEG/IEM resin with 30% and 40% plasticizer content are shown in Figure S2, Supporting Information. The test results show that the  $T_g$  drop is not obvious, but the modulus decreases obviously, and it is of little significance to add the plasticizer. The mechanical properties of the PEG/IEM resin decrease significantly with increasing temperature. The strength of the PEG/IEM resin at the  $T_g$  is very weak, and the stent is not enough to support the ureter. Therefore, the  $T_g$  of the PEG/IEM resin is higher than the human body temperature (about 37 °C). In addition, the physiological temperature is not always stable. The stent with the  $T_g$  of 44 °C can also have excellent mechanical properties under special human conditions, such as fever. So the selection of a 30% mass fraction of plasticizer is the relatively appropriate choice.

## 2.2. Shape Memory Performance of PEG/IEM Resin

In this paper, the shape recovery behavior of the UV-cured PEG/IEM resin was analyzed and demonstrated at the macro and micro levels. Macroscopically, the U-shaped UV-cured PEG/IEM resin samples were driven and recovered by the heating table and hot water; Microscopically, the shape memory properties of the UV-cured PEG/IEM resin samples were tested by the DMA cycle method test.

Figure S3 and Figure S4, Supporting Information, show the U-shaped samples shape recovery process of the UV-cured PEG/IEM resins with different molecular weights of raw PEG ( $M_n=4000, 6000, \text{ and } 8000$ ) and their plasticized resins during recovery on the 90 °C heating table. According to the results, with the increase of raw PEG molecular weight, the time required for shape recovery of the resins became longer. The time required for the UV-cured PEG/IEM resins with raw PEG molecular weight of 4000, 6000, and 8000 to recover to the initial shape was 95, 240, and 295, respectively (Figure S3, Supporting Information). At the same time, the addition of a plasticizer could significantly reduce the time required for shape recovery. After plasticized by 30wt% triacetate, the time required for the UV-cured PEG/IEM resins with raw PEG molecular weights of 4000, 6000, and 8000

to return to the initial shape was decreased to 75, 95, and 240s, respectively (Figure S4, Supporting Information).

In addition, when the UV-cured PEG/IEM resins recovered shape in the water, it can be realized that the shape recovery angle is over 180° under the action of water driving. This is because the UV-cured PEG/IEM resin specimens had different crosslinking gradients in the thickness direction under unilateral UV curing, resulting in a capacity gradient in the water absorption performance. Under the action of this gradient, the UV-cured cured PEG/IEM resins could realize water-driven deformation over 180°.

Using the stress-strain test method of the DMA tensile module, the shape memory cycle performance of the UV-cured PEG/IEM resins was tested at the micro level. The specific test process was described above. The shape memory cycle curves of the UV-cured PEG/IEM resins with different molecular weights of raw PEG ( $M_n=4000, 6000, \text{ and } 8000$ ) were separately shown in Figure 4a–c. The shape recovery rate of the resin can be calculated by dividing the difference between post-tensile strain and post-recovery strain of two adjacent times. According to the curves, the shape recovery rate of the resins can be obtained twice. It can be seen that the shape deformation of the resins increases with the increase of molecular weight of raw PEG.

The comprehensive test results of the above three figures are shown in Figure 4d. In the DMA test, the shape recovery rate ( $R_r$ ) is calculated twice. Take Figure 4a as an example, the  $R_r$  of the first cycle is calculated by  $(Y_3 - Y_2) / (Y_2 - Y_1)$ . The  $R_r$  of the second cycle is calculated by  $(Y_5 - Y_4) / (Y_4 - Y_3)$ . The shape recovery rate of the UV-cured PEG/IEM resin increased with the increase of raw PEG molecular weight. At the same time, the shape recovery rate of the second cycle is higher than that of the first. The minimum shape recovery rate could also reach more than 94% so that the shape recovery rate of the UV-cured PEG/IEM resins was high enough to meet the requirements of the biological application.

Figure 5 shows the shape recovery process of the butterfly made by the PEG4000/IEM resin. The process was carried out in an oven at 90 °C and the unfolding process of butterfly wings from 90° to 180° took 40 s demonstrating excellent shape recovery performance of the PEG4000/IEM resin.

## 2.3. Cytotoxicity of PEG/IEM Resin

The cytocompatibility of PEG resin was tested by the cytotoxicity test. As described previously, the cytotoxicity of the UV-cured PEG/IEM resin was determined by the live/dead staining (cell coculture) method. The co-culture experiments of cells and materials were carried out indirectly in a culture medium. In this text, cells were inoculated with a 24-well plate, and then the transwell was placed on the 24-well plate. The PEG/IEM resin was placed in the transwell, and 1 mL medium was added to the culture for 5 days for staining. Fibroblasts were co-cultured with the UV-cured PEG/IEM resin extract for 5 days. The fluorescent images are shown in Figure 6. After one day, the cell density was relatively low, and no obvious dead cells were observed. After three days, the cell number increases significantly. Compared with the cell culture of the blank group, the cells of the PEG/IEM group grew normally with good morphology and no obvious

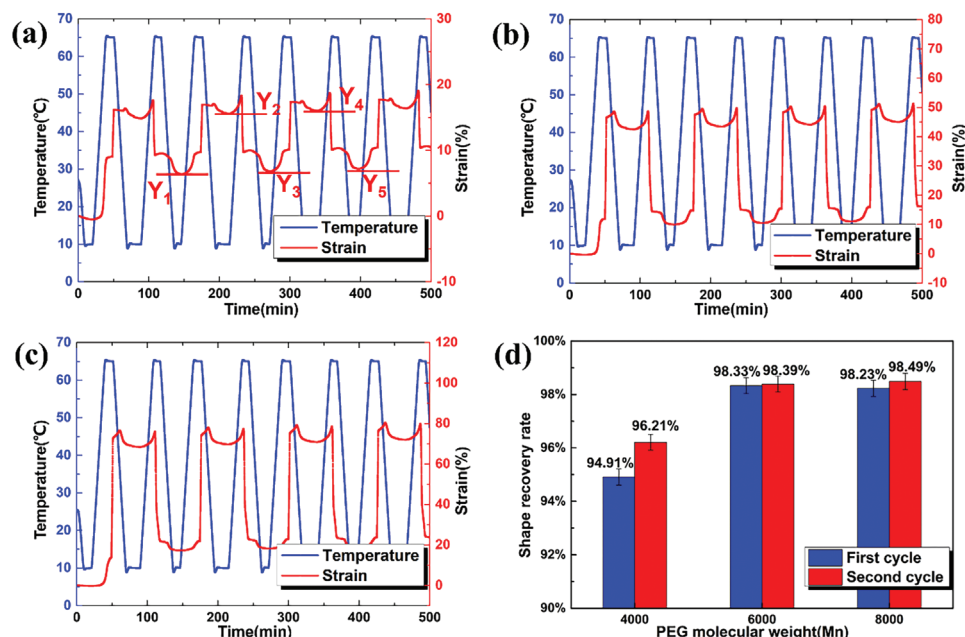


**Figure 4.** Shape memory cycle test curves of the UV-cured PEG/IEM resins with raw PEG molecular weight of a) 4000, b) 6000, and c) 8000 and d) histogram of comprehensive test results of the UV-cured PEG/IEM resins.

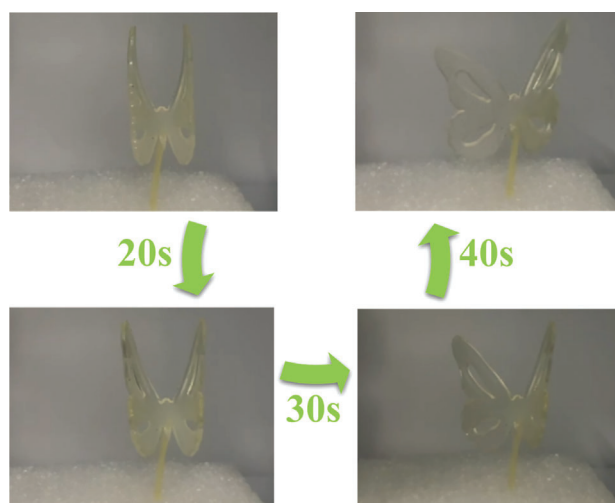


**Figure 5.** The unfolding of the butterfly wings based on UV-cured PEG4000/IEM resin.

death, indicating that UV-cured PEG/IEM resin had no cytotoxicity and good biosafety. It provided a basic prospect for the in vivo verification and biological application of the UV-cured PEG/IEM resin devices.

## 2.4. Characterization of $\text{Fe}_3\text{O}_4/\text{PEG4000}/\text{IEM}$ Resin Composite

**Figure 7** is the cross-sectional SEM image of the prepared 10wt% nano  $\text{Fe}_3\text{O}_4/\text{PEG4000}/\text{IEM}$  resin composite. It could be seen in **Figure 7a** that although nano  $\text{Fe}_3\text{O}_4$  was slightly agglomerated, the overall distribution was relatively uniform. The pores in the

resin matrix were formed during the curing process of the resin, which provided a structural basis for the water absorption and water-driven shape memory properties of the resin. The cracks in the resin matrix were formed during the SEM test, which was caused by the instantaneous and significant temperature rise of the resin surface due to secondary electron irradiation. **Figure 7b** is a local magnified SEM image of the red box part in **Figure 7a**. The resin had good encapsulation of nano  $\text{Fe}_3\text{O}_4$ .

The prepared UV-cured PEG4000/IEM/ $\text{Fe}_3\text{O}_4$  resin composite properties were tested and compared with those of the UV-cured PEG4000/IEM resin. The results are shown in **Figure 8**. DSC test results in **Figure 8a** showed that after adding 10wt% nano  $\text{Fe}_3\text{O}_4$  to the UV-cured PEG4000/IEM resin, the semi-crystalline melting temperature of the composite decreased from 52.9 to 47.5 °C. The addition of nano  $\text{Fe}_3\text{O}_4$  destroyed the regularity of the semi-crystalline structure in the UV-cured PEG4000/IEM resin, which led to a decrease in the semi-crystalline melting temperature of the composite. The static tensile test results in **Figure 8b** showed that the elastic modulus of the composite decreased from 359.6 to 114.9 MPa (strain 0.01) at room temperature compared with the UV-cured PEG4000/IEM resin. However, the composite showed a high elastic deformation stage that the UV-cured PEG4000/IEM resin did not have at room temperature. Nano  $\text{Fe}_3\text{O}_4$  as a nano rigid inorganic particle filling material has a large specific surface area and good compatibility with resin. These characteristics play an excellent role in absorbing energy so that the toughness of the UV-cured PEG4000/IEM/ $\text{Fe}_3\text{O}_4$  resin composite can be significantly enhanced under the action of tensile stress.  $\text{Fe}_3\text{O}_4$  particles in the PEG resin matrix impede the movement of the PEG molecular chain. The blocking effect is becoming more and more obvious with the increasing  $\text{Fe}_3\text{O}_4$ , resulting in the decline of crystallinity, which makes the modulus and  $T_m$  of the composites show a downward trend. **Figure 8b**

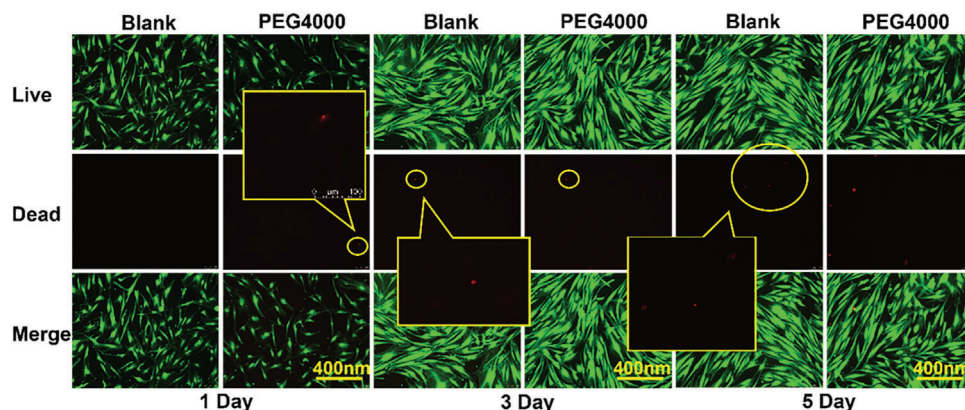


**Figure 6.** Fluorescent images of the fibroblasts cells cultured in PEG/IEM resin (PEG of  $M_n=4000$ ) for 1, 3, and 5 days (Living cells: green; dead cells: red).

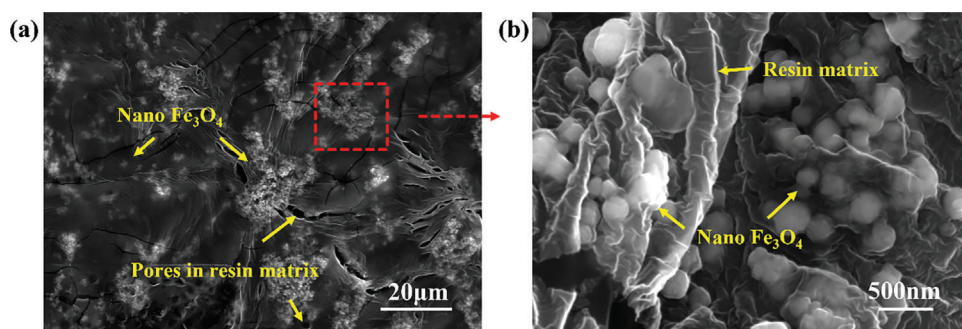


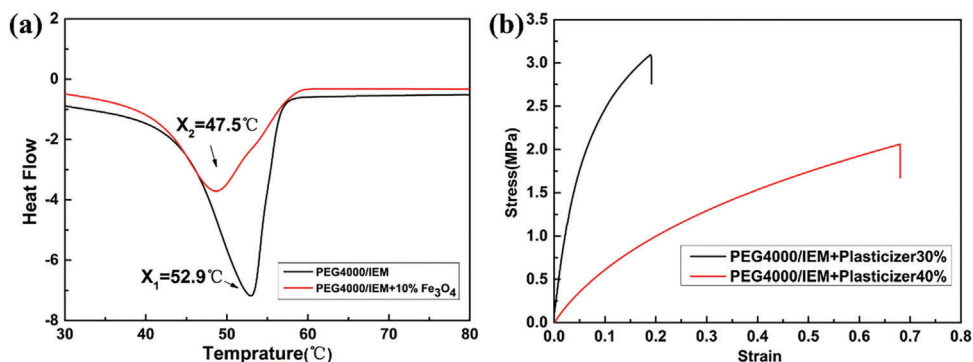
**Figure 7.** a) Cross-sectional SEM image of the 10wt% nano  $Fe_3O_4$ /PEG4000/IEM resin composite; b) Local magnified SEM image of the red box part.

shows the mass fraction of nano  $Fe_3O_4$  is 10%. Therefore, when the temperature reaches  $T_{trans}$ , the modulus of the material decreases significantly.

10wt% nano  $Fe_3O_4$ /PEG4000/IEM resin composite spring stent structure was prepared. The temporary shape was obtained by stretching at  $60^\circ C$  and then cooling to room temperature. The potential application scenario of composite spring is shown in **Figure 9a**. The shape recovery process (Figure 9b) and shape recovery temperature change (Figure 9c) of the spring stent structure under a magnetic field were studied. An Infracam hr. infrared thermal imager obtained the shape recovery tempera-

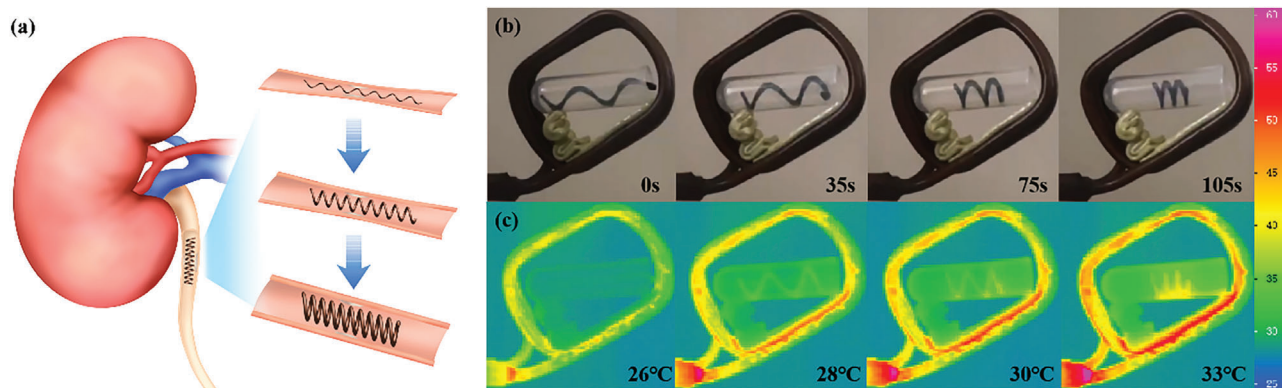
ture change. The temperature range of thermal imaging was  $25-60^\circ C$ . The infrared thermal imaging colors corresponding to different temperatures are shown in the ruler on the right side of Figure 9b.

Figure 9b shows that the shape recovery of the spring stent structure took 105s. The shape of the spring stent structure was completely and quickly recovered, and the shape memory performance was excellent. As is shown in Figure 9c, the spring stent structure was difficult to be observed in the infrared image at the beginning. The spring stent structure gradually became visible with the increase in temperature due to the friction



**Figure 8.** a) DSC curves of the UV-cured PEG/IEM resin and 10wt% nano  $Fe_3O_4$ /PEG/IEM resin composite (PEG of  $M_n=4000$ ); b) Stress-strain curves of the UV-cured PEG/IEM resin and 10wt% nano  $Fe_3O_4$ /PEG/IEM resin composite (PEG of  $M_n=4000$ ).





**Figure 9.** a) Application scenario, b) shape recovery process, and c) shape recovery temperature change of 10wt% nano  $\text{Fe}_3\text{O}_4$ /PEG/IEM resin composite spring stent structure under a magnetic field (PEG of  $M_n=4000$ ).

caused by internal nano  $\text{Fe}_3\text{O}_4$  vibration. It could be seen that the shape recovery of the composite spring stent structure did not need much high temperature. At the end of the shape recovery process, the lowest temperature detected on the spring stent structure was only 33 °C. Although the temperature may only be the temperature of the stent surface, it still indicates that the stent structure is expected to be used close to or lower than the human body temperature. Relying on the human body temperature, the stent can automatically complete the deployment in the human body. Magnetic-driven shape recovery test indicated that PEG/IEM resin and its nano  $\text{Fe}_3\text{O}_4$  composite have potential application prospects in the biological stent.

In addition, utilizing ABAQUS software, we simulate the development process of the spring stent. By comparison with the experiment, the two results are consistent. Using ABAQUS software, the shape memory behavior of 10wt% nano  $\text{Fe}_3\text{O}_4$ /PEG4000/IEM resin composite was simulated by uniaxial tension. Four steps were set in the process of simulating: 1) applied a temperature load to the composite above the glass transition temperature and then applied a tensile deformation of 20 mm to the composite; 2) kept the deformation of the composite unchanged at high temperature and gradually cooled down to below the glass transition temperature; 3) When the temperature was reduced to room temperature, the applied load was removed, and the temporary shape of the SMP remained unchanged; 4) the composite was heated above the glass transition temperature again, then the composite returned to the initial state. The model size used was 8mm×5mm×5 mm, which was consistent with the experimental size. The model used is shown in Figure S5, Supporting Information. The simulation results in Figure S5, Supporting Information, were consistent with the experimental results in Figure 9. The experimental parameters used in the simulation of shape recovery are shown in Table S1 and Table S2, Supporting Information.

### 3. Conclusions

The UV-cured PEG/IEM resins with different molecular weights of raw PEG were prepared, and the  $T_{\text{trans}}$  of the resin was adjusted to 44 °C by plasticizers to make it closer to the human body temperature. Cytotoxicity and DMA shape memory cycle tests showed that the resins have excellent biosafety and shape

memory performances. The mechanical property of the resins met the soft material required by the biological stent and could be cured rapidly under UV light. 10wt% nano  $\text{Fe}_3\text{O}_4$ /PEG4000/IEM resin composite and its spring stent structure were prepared and tested. The stent structure can quickly recover to the original shape for 105s under magnetically driven with excellent comprehensive performance. It provides a material basis and forming method for developing a new intestinal stent or ureter stent. It can be predicted that different biological application scenarios can be met by adding other functional materials to the prepared resins so that the UV-cured PEG/IEM resins and their composites have potential application value in imaging, multiple driving modes, photodynamic therapy, and so on.

### 4. Experimental Section

**Materials:** PEG ( $M_n = 4000, 6000, \text{ and } 8000$ ) and IEM as raw material, triacetin as the plasticizer, stannous octoate  $[\text{Sn}(\text{Oct})_2]$  as the catalyst, and Diphenyl(2,4,6-trimethyl benzoyl)phosphine oxide (TPO) as the photoinitiator were all purchased from Aladdin.

**Synthesis of PEG/IEM Resin:** PEG was first dried under vacuum at 120 °C for 3 h using a heating table, then the dried PEG and  $\text{Sn}(\text{Oct})_2$  (mole ratio 100:1) were added into a three-neck flask in an oil bath at 65 °C under nitrogen, IEM (2:1 mole ratio to PEG) was then slowly added dropwise with the syringe. The reaction proceeded under nitrogen protection and stirred for 1.5 h. The reaction product was soaked in ethanol for 24 h to remove unreacted small molecule residues.

**Preparation of UV Cured PEG/IEM Resin and Plasticized UV Cured PEG/IEM Resin:** TPO was added to the synthesized PEG/IEM resin as a photoinitiator; the amount of TPO was 0.02% of the resin mass. The mixture was stirred on a heating table at 70 °C for 5 min to homogeneous dissolve TPO. The mixture was poured into a transparent mold preheated to 70 °C in advance. The resin was then cured under 405 nm ultraviolet light for 5 min in the UV curing device (Anycubic Wash&Cure Plus). The cured PEG resin sample can be obtained after cooling and demolding. When preparing plasticized resin sample, PEG/IEM resin was mixed with triacetin in the ratio of 7:3, and processed as described in the previous steps (the amount of TPO was 0.02% of the total mass of mixed resin).

**Thermal Analysis:** Differential scanning calorimetry (DSC) was used to investigate the thermal properties dominated by the transition temperature of the cured PEG/IEM resin and the cured plasticized resin. The instrument was Mettler Toledo DSC1. The sample was 5–10 mg powder filed with a file. The test temperature ranged from 25 to 100 °C at the rate of 5 °C  $\text{min}^{-1}$ . The test was carried out in a nitrogen atmosphere. The heating and cooling cycles went twice to eliminate the influence of heat history.



The second temperature rise curve was taken as the test result. Thermal gravimetric analysis (TGA) was used to study the quality change of the cured PEG/IEM resin with temperature by Mettler Toledo TGA/DSC1. The sample was 10–15 mg powder filed with a file. The test temperature ranged from 30 to 800 °C at the rate of 10 °C min<sup>-1</sup>. The test was carried out in a nitrogen atmosphere.

**Shape Memory Properties Analysis:** Dynamic mechanical and thermal analysis was used to test the shape memory performance of the cured PEG/IEM resin under dynamic cycles by the TA Q800 instrument (tensile mode, 5 Hz frequency). The test specimen was a rod of 30×5×1 mm<sup>3</sup>. Test temperature equilibrated at 10 °C isothermals for 10.00 min and raised to 65 °C by the rate of 3 °C min<sup>-1</sup> isothermal for 10.00 min. Then a 0.5–1N force was loaded onto the test specimen. The test temperature was then decreased to 10 °C at the rate of –3 °C min<sup>-1</sup> isothermal for 10.00 min. Unloaded the force for 10 min, then raised the temperature to 65 °C at the rate of 3 °C min<sup>-1</sup> again. Thus a shape memory cycle was completed. The test temperature was decreased again to start the next two cycles to study the repeatability of shape memory performance of the cured PEG/IEM resin. Apparent shape memory performance was tested by shape fixed and shape recovery of U-shaped specimens. A self-made mold molded the U-shaped specimen; the fixed angle after demolding was taken as the shape fixity angle ( $\theta_f$ ); the recovery angle after the heating specimen was taken as the shape recovery angle ( $\theta_r$ ). The shape fixity rate ( $R_f$ ) and the shape recovery rate ( $R_r$ ) can be expressed by Equations (1) and (2).

$$R_f = \frac{180^\circ - \theta_f}{180^\circ} \times 100\% \quad (1)$$

$$R_r = \frac{\theta_r - \theta_f}{180^\circ - \theta_f} \times 100\% \quad (2)$$

**Mechanical Property Analysis:** Tensile mechanical property test was used to study the stress-strain property of the cured PEG/IEM resin with a Zwick/roell universal testing machine. The test was carried out according to ASTM D638, the maximum range of 10 kN, and the strain was determined by a displacement extensometer. The tensile specimen was shaped dumbbell taken from the polymer plate by laser cutting referring to ASTM D638, type IV standard. The tensile was carried out at room temperature (25 °C) at the rate of 10 mm min<sup>-1</sup>. The tensile property at different temperatures was also investigated.

**Biocompatibility Test:** Cytotoxicity test was conducted by GB/T16886.5-2003, Standard biological evaluation of medical devices Part 5: Test for in vitro cytotoxicity. The cytotoxicity of PEG/IEM resin was measured by live/dead staining (cells coculture). Fibroblasts were cocultured with PEG/IEM resin extractive for 5 days. The cytotoxicity of PEG/IEM resin was obtained by comparing the cell culture of the control group.

## Supporting Information

Supporting Information is available from the Wiley Online Library or from the author.

## Acknowledgements

This work was supported by the National Key R&D Program of China (Grant No. 2022YFB3805700) and the National Natural Science Foundation of China (Grant No. 12072094). The authors thank Lu Wang, Shuai Yang, and Lan Luo for their kind help.

## Conflict of Interest

The authors declare no conflict of interest.

## Data Availability Statement

The data that support the findings of this study are available from the corresponding author upon reasonable request.

## Keywords

composites, shape memory poly(ethylene glycol)/isocyanatoethyl methacrylate resin, ureter stents, UV-curing

Received: February 7, 2023

Revised: April 12, 2023

Published online:

- [1] L. Liverani, A. Liguori, P. Zezza, C. Gualandi, M. Toselli, A. R. Boccacini, M. L. Focarete, *Bioact. Mater.* **2022**, *11*, 230.
- [2] A. Gupta, T. H. Mekonnen, *J. Colloid Interface Sci.* **2022**, *611*, 726.
- [3] L. Luo, F. Zhang, W. Pan, Y. Yao, Y. Liu, J. Leng, *Smart Mater. Struct.* **2022**, *31*, 035008.
- [4] Y. Qi, B. Gu, B. Sun, W. Zhang, *Compos. Sci. Technol.* **2022**, *219*, 109250.
- [5] L. Chen, Y. Zhang, Z. Liu, Q. Song, C. Liu, *Mater. Today Commun.* **2022**, *30*, 103025.
- [6] X. Sun, Z. Zhang, Z. Sun, J. Zheng, X. Liu, H. Xia, *Macromol. Rapid Commun.* **2022**, *43*, 2100863.
- [7] P. Zhang, F. Cai, G. Wang, H. Yu, *Chin. J. Polym. Sci.* **2022**, *40*, 166.
- [8] A. Cortés, N. Pérez-Chao, A. Jiménez-Suárez, M. Campo, S. G. Prolongo, *Eur. Polym. J.* **2022**, *164*, 110888.
- [9] Z. Liu, S. Hao, X. Lan, W. Bian, L. Liu, Q. Li, Z. Fu, Y. Liu, J. Leng, *Smart Mater. Struct.* **2022**, *31*, 025021.
- [10] J. Zhang, C. Zhang, F. Song, Q. Shang, Y. Hu, P. Jia, C. Liu, L. Hu, G. Zhu, J. Huang, Y. Zhou, *Chem. Eng. J.* **2022**, *429*, 131848.
- [11] X. Wang, Y. He, J. Leng, *Macromol. Mater. Eng.* **2022**, *43*, 2100863.
- [12] J. Yang, J. Gong, L. Tao, Z. Tang, Z. Yang, P. Cao, Q. Wang, T. Wang, H. Luo, Y. Zhang, *Polym. J.* **2022**, *54*, 697.
- [13] X. Chen, S. Han, W. Wu, Z. Wu, Y. Yuan, J. Wu, C. Liu, *Small* **2022**, *18*, 2106824.
- [14] C. Zhang, X. Lu, Z. Wang, H. Xia, *Macromol. Rapid Commun.* **2022**, *43*, 2100768.
- [15] X. Chen, R. Wang, C. Cui, L. An, Q. Zhang, Y. Cheng, Y. Zhang, *Chem. Eng. J.* **2022**, *428*, 131212.
- [16] C. Zeng, L. Liu, W. Bian, J. Leng, Y. Liu, *Compos. Struct.* **2022**, *280*, 114952.
- [17] Y. Yang, L. Huang, R. Wu, Z. Niu, W. Fan, Q. Dai, L. Cui, J. He, C. Bai, *ACS Appl. Mater. Interfaces* **2022**, *14*, 3344.
- [18] L. Qiao, C. Liu, C. Liu, L. Zong, H. Gu, C. Wang, X. Jian, *Eur. Polym. J.* **2022**, *162*, 110838.
- [19] C. Lin, L. Liu, Y. Liu, J. Leng, *Compos. Struct.* **2022**, *279*, 114729.
- [20] K. Hashimoto, N. Kurokawa, A. Hotta, *Polymer* **2021**, *233*, 124190.
- [21] M. H. Moghim, S. M. Zebarjad, R. Egra, *J. Polym. Res.* **2022**, *29*, 28.
- [22] A. Babaie, M. Rezaei, H. Roghani-Mamaqani, *Macromol. Mater. Eng.* **2022**, *307*, 2100637.
- [23] W. Wang, Z. Guo, Z. Liu, S. Qiu, C. Li, Q. Zhang, *Polym. Chem.* **2021**, *12*, 5851.
- [24] B. Kurt, U. Gulyuz, D. D. Demir, O. Okay, *Eur. Polym. J.* **2016**, *81*, 12.
- [25] C. Lin, J. Lv, Y. Li, F. Zhang, J. Li, Y. Liu, L. Liu, J. Leng, *Adv. Funct. Mater.* **2019**, *29*, 1906569.
- [26] J. Kuroviak, A. Mackiewicz, T. Klekiel, R. Bedzinski, *Materials* **2022**, *15*, 1225.
- [27] T. L. Hill, A. C. Berent, C. W. Weisse, *J. Vet. Intern. Med.* **2014**, *28*, 1384.
- [28] E. Palminteri, M. Gacci, E. Berdondini, M. Poluzzi, G. Franco, V. Gentile, *Eur. Urol.* **2010**, *57*, 615.

- [29] W. Hu, Y. Song, Y. Li, Y. Li, J. Mu, X. Zhong, Y. Chen, R. Wu, Y. Xiao, C. Huang, *Sci. Rep.* **2021**, *11*, 22358.
- [30] S. T. Ahn, D. H. Lee, J. W. Kim, D. G. Moon, *J. Clin. Med.* **2020**, *9*, 1274.
- [31] J. C. Kim, Y. W. Chang, M. Sabzi, *Eur. Polym. J.* **2021**, *152*, 110488.
- [32] S. M. Lai, J. L. Liu, Y. H. Huang, *J. Macromol. Sci., Part B: Phys.* **2020**, *59*, 587.
- [33] F. Wang, C. Zhang, A. Tan, H. Chen, S. Weng, Q. Xie, C. Li, Z. Cai, X. Wan, *Polymer* **2021**, *223*, 123677.
- [34] A. Fulati, K. Uto, M. Iwanaga, M. Ebara, *Adv. Healthcare Mater.* **2022**, *11*, 2200050.
- [35] M. Liu, M. Shafiq, B. Sun, J. Wu, W. Wang, M. EL-Newehy, H. EL-Hamshary, Y. Morsi, O. Ali, A. ur Rehman Khan, X. Mo, *Adv. Healthcare Mater.* **2022**, *11*, 2200499.
- [36] K. L. Wiley, B. P. Sutherland, B. A. Ogunnaike, A. M. Kloxin, *Adv. Healthcare Mater.* **2022**, *11*, 2101947.
- [37] K. Luo, L. Wang, J. Tang, X. Zeng, X. Chen, P. Zhang, S. Zhou, J. Lia, Y. Zuo, *J. Mater. Chem. B* **2021**, *9*, 9191.
- [38] W. Feng, Y. Zhang, Y. Shao, T. Huang, N. Zhang, J. Yang, X. Qi, Y. Wang, *Eur. Polym. J.* **2021**, *145*, 110245.
- [39] S. Jafari, M. Nourany, M. Zakizadeh, A. Taghilou, H. A. Ranjbar, *Etoiles Compos. Chim. Anorm. Debut Sequence Princ., Commun. Colloq. Int. Astrophys., 23rd* **2020**, *19*, 194.